A BAYESIAN PROBABILISTIC DAMAGE DETECTION USING LOAD-DEPENDENT RITZ VECTORS

HOON SOHN [*] and KINCHO H. LAW [†]

Department of Civil and Environmental Engineering, Stanford University, Stanford, CA 94305-4020, U.S.A.

ABSTRACT

This paper demonstrates the possibility of incorporating load-dependent Ritz vectors, as an alternative to modal parameters, into a Bayesian probabilistic framework for detecting damages in a structure. Recent research has shown that it is possible to extract load-dependent Ritz vectors from vibration tests [2]. This paper shows that load-dependent Ritz vectors have the following potential advantages for damage detection over modal vectors: (1) In general, load-dependent Ritz vectors are more sensitive to damage than the corresponding modal vectors, and (2) substructures of interest can be made more observable using the load-dependent Ritz vectors generated from particular load patterns. An eight-bay truss example is presented to illustrate the applicability of the proposed approach.

1 INTRODUCTION

One common approach for global damage detection is to employ the vibration characteristics of a structure such as frequencies, modal vectors, and modal damping to predict the damage locations and to estimate the amount of damage. However, it has been shown that changes in the modal parameters might not be apparent at an early stage of damage. Also, the uncertainties caused by measurement noise, modeling error involved in an analytical model, and environmental changes such as variations in temperature and load conditions can impede the reliable identification of damage. Therefore, for reliable damage detection, the damage would need to cause significant changes in the modal parameters that are beyond the natural variability caused by the effects other than the damage.

Recent research has shown that it is possible to extract Ritz vectors from vibration tests [2]. The first Ritz vector is the static deformation of a structure due to a particular load applied to the structure. The subsequent vectors account for the inertial effects of the loading and are generated by iterative matrix multiplication and orthogonalization. Ritz vectors (or Lanczos vectors) have been shown very effective for dynamic and earthquake analyses, eigenvalue problems and model reductions. In this paper, we demonstrate the possibility of incorporating load-dependent Ritz vectors, as an alternative to modal

parameters, into the previously proposed Bayesian probabilistic framework for damage detection [5]. This study is motivated by the following potential advantages of Ritz vectors over modal vectors: (1) In general, Ritz vectors are more sensitive to damage than the corresponding modal vectors, (2) substructures of interest can be made more observable using the Ritz vectors generated from particular load patterns, (3) the computation of Ritz vectors is less expensive than that of modal vectors (eigenvectors) and (4) while the practical difficulties of modal testing impede the extraction of a large number of meaningful modes, a larger number of Ritz vectors can be extracted by imposing different load patterns on a structure.

This paper is organized as follows: The next section reviews the theoretical formulation of the previously proposed Bayesian probabilistic approach [5]. Section 3 presents numerical examples to illustrate the effectiveness of the proposed method. Section 4 summarizes this paper.

2 THEORETICAL FORMULATION

Bayesian probabilistic approaches, which use modal parameters, have been applied to damage detection by researchers [1, 5]. The idea is to search for the most probable damage event by comparing the relative probabilities for different damage scenarios, where the relative probability of a damage event is expressed in terms of the posterior probability of the damage event, given the estimated modal data sets from a structure. In this paper, the formulation of the relative posterior probability is based on an output error, which is defined as the difference between the estimated Ritz vectors and the theoretical Ritz vectors from the analytical model.

2.1 Notations and Assumptions

For an analytical model of a structure, we represent the system stiffness matrix $\mathbf{K}$ as an assembly of substructure stiffness matrices. For a model with N_{sub} substructures, the overall stiffness matrix can be expressed as:

$$\mathbf{K}(\Theta) = \sum_{i=1}^{N_{sub}} \theta_i \mathbf{K}_{si} \qquad (1)$$

where $\mathbf{K}_{si}$ is the stiffness matrix of the ith substructure and θ_i $(0 \leq \theta_i \leq 1)$ is a nondimensional parameter which represents the contribution of the ith substructure

*Graduate Student, email: sohnhoon@leland.stanford.edu
†Professor, email: law@ce.stanford.edu

stiffness to the system stiffness matrix. The nondimensional parameter θ_i is introduced to allow the modeling of damage in the ith substructure. A substructure is defined as *damaged* when the θ value is less than a specified threshold. As damage locations and amount are determined according to the θ values, the system stiffness matrix in Equation (1) is expressed as a function of $\Theta = \{\theta_i; i = 1, ..., N_{sub}\}$.

Test data sets are assumed to be collected from repeated vibration tests. When vibration tests are repeated N_s times, the total collection of N_s data sets is denoted as:

$$\hat{\Psi}_{N_s} = \{\hat{\psi}(n) \ : \ n = 1, ..., N_s\} \tag{2}$$

A data set $\hat{\psi}(n)$ in Equation (2) is composed of Ritz vectors estimated from the nth vibration test:

$$\hat{\psi}(n) = \left[\hat{\mathbf{r}}_1^{nT}, ..., \hat{\mathbf{r}}_{N_r}^{nT}\right]^T \in \mathbf{R}^{N_t} \tag{3}$$

where $\hat{\mathbf{r}}_i^n$ denotes the ith estimated Ritz vector in the nth data set. The Ritz vector $\hat{\mathbf{r}}_i^n$ ($\hat{\mathbf{r}}_i^n \in \mathbf{R}^{N_d}$) has components corresponding to the instrumented degrees of freedom (DOFs). The variables N_t, N_d and N_r represent the total number of components in a data set $\hat{\psi}(n)$, the number of the measured DOFs and the number of the estimated Ritz vectors, respectively.

Let H_j denote a hypothesis for a damage event which can contain any number of substructures as damaged, and the initial degree of belief about the hypothesis H_j is represented with a prior probability $P(H_j)$. Using Baye's theorem, the posterior probability $P(H_j|\hat{\Psi}_{N_s})$, after observing the estimated data sets $\hat{\Psi}_{N_s}$, is given as:

$$P(H_j|\hat{\Psi}_{N_s}) = \frac{P(\hat{\Psi}_{N_s}|H_j)}{P(\hat{\Psi}_{N_s})} P(H_j) \tag{4}$$

The most likely damaged substructures are the ones included in the hypothesis H_{max} which has the largest posterior probability, i.e.

$$P(H_{max}|\hat{\Psi}_{N_s}) = \max_{\forall H_j} P(H_j|\hat{\Psi}_{N_s}) \tag{5}$$

Since the objective is to determine the most probable damage hypothesis (event), only the relative posterior probabilities of alternative hypotheses are of interest. We attempt to avoid the explicit expression of a posterior probability $P(H_j|\hat{\Psi}_{N_s})$ since the precise calculation of $P(\hat{\Psi}_{N_s}|H_j)$ is a difficult task. To overcome these difficulties, we focus on the relative comparisons of posterior probabilities.

2.2 Determination of the Most Probable Damage Event

When applying Equation (4) to calculate the posterior probability $P(H_j|\hat{\Psi}_{N_s})$, the only undefined term is $P(\hat{\Psi}_{N_s}|H_j)$. The prior probability of a hypothesis $P(H_j)$

is the prior information given by users and the probability of estimated test data $P(\hat{\Psi}_{N_s})$ is simply a normalizing constant.

As shown in Equation (1), less than a unity value for θ_i reflects the stiffness decrease in the ith substructure. As noted earlier, damage is characterized by stiffness reduction. When θ_i is less than a specified threshold $\theta_i^*(< 1)$, the ith substructure is defined as *damaged*. If we define $\Theta_{H_j}^1$ as a set of θ_i's corresponding to the damaged substructures in a hypothesis H_j and $\Theta_{H_j}^2$ as the remaining θ_i's, the conditional probability $P(\hat{\Psi}_{N_s}|H_j)$ can be interpreted as the probability of obtaining $\hat{\Psi}_{N_s}$ when the θ_i's in $\Theta_{H_j}^1$ are less than or equal to their threshold θ_i^*'s and the remaining θ_i's stay within $\theta_i^* < \theta_i \leq 1$. Denoting $\Omega_{H_j}^*$ as the range of Θ_{H_j} such that $0 \leq \Theta_{H_j}^1 \leq \Theta_{H_j}^{1,*}$ and $\Theta_{H_j}^{2,*} < \Theta_{H_j}^2 \leq 1$, the conditional probability $P(\hat{\Psi}_{H_j}|H_j)$ becomes:

$$P(\hat{\Psi}_{N_s}|H_j) = P(\hat{\Psi}_{N_s}|\Theta_{H_j} < \Omega_{H_j}^*)$$

$$= \frac{P(\Theta_{H_j} < \Omega_{H_j}^* |\hat{\Psi}_{N_s}) \, P(\hat{\Psi}_{N_s})}{P(\Theta_{H_j} < \Omega_{H_j}^*)}$$

$$= \frac{P(\hat{\Psi}_{N_s})}{P(\Theta_{H_j} < \Omega_{H_j}^*)} \int_{\Theta_{H_j} < \Omega_{H_j}^*} f(\Theta_{H_j}|\hat{\Psi}_{N_s}) d\Theta_{H_j} \tag{6}$$

where $\Theta_{H_j}^{1,*}$ and $\Theta_{H_j}^{2,*}$ are the sets of damage thresholds for $\Theta_{H_j}^1$ and $\Theta_{H_j}^2$, respectively, and $f(\Theta_{H_j}|\hat{\Psi}_{N_s})$ is a conditional probability density function (PDF) of Θ_{H_j} given $\hat{\Psi}_{N_s}$. Furthermore, $\Theta_{H_j} < \Omega_{H_j}^*$ indicates that Θ_{H_j} are within the range of $\Omega_{H_j}^*$ such that $0 \leq \Theta_{H_j}^1 \leq \Theta_{H_j}^{1,*}$ and $\Theta_{H_j}^{2,*} < \Theta_{H_j}^2 \leq 1$.

If we define the most probable parameter values $\Theta_{H_j}^{max}$, given a hypothesis H_j, such that:

$$f(\Theta_{H_j}^{max}|\hat{\Psi}_{N_s}) = \max_{\Theta_{H_j} < \Omega_{H_j}^*} f(\Theta_{H_j}|\hat{\Psi}_{N_s}) \tag{7}$$

then the upper bound of $P(\hat{\Psi}_{N_s}|H_j)$ in Equation (6) becomes:

$$P_U(\hat{\Psi}_{N_s}|H_j) \tag{8}$$

$$= \frac{P(\hat{\Psi}_{N_s})}{P(\Theta_{H_j} < \Omega_{H_j}^*)} \int_{\Theta_{H_j} < \Omega_{H_j}^*} f(\Theta_{H_j}^{max}|\hat{\Psi}_{N_s}) d\Theta_{H_j}$$

$$= \frac{P(\hat{\Psi}_{N_s})}{P(\Theta_{H_j} < \Omega_{H_j}^*)} f(\Theta_{H_j}^{max}|\hat{\Psi}_{N_s}) \int_{\Theta_{H_j} < \Omega_{H_j}^*} 1 \, d\Theta_{H_j}$$

For simplification, we assume that if damage occurs, it can have any arbitrary amount with equal probability. That is, we assign a uniform probability density function to θ_i such that:

$$f(\theta_i) = \begin{cases} 1 & \text{if } 0 \leq \theta_i \leq 1 \\ 0 & \text{otherwise} \end{cases} \tag{9}$$

Furthermore, if θ_i's are assumed to be independent, the following two equations hold:

$$f(\Theta_{H_j}) = \prod_{\forall\, \theta_i \in \Theta_{H_j}} f(\theta_i) = 1 \qquad (10)$$

$$\frac{1}{P(\Theta_{H_j} < \Omega_{H_j}^*)} = \frac{1}{\int_{\Theta_{H_j} < \Omega_{H_j}^*} f(\Theta_{H_j}) d\Theta_{H_j}}$$
$$= \frac{1}{\int_{\Theta_{H_j} < \Omega_{H_j}^*} 1\, d\Theta_{H_j}} \qquad (11)$$

Substituting Equation (11) into Equation (8), $P_U(\hat{\Psi}_{N_s}|H_j)$ can be simplified as:

$$P_U(\hat{\Psi}_{N_s}|H_j) = f(\Theta_{H_j}^{max}|\hat{\Psi}_{N_s})\, P(\hat{\Psi}_{N_s}) \qquad (12)$$

The next step is to compute the conditional PDF, $f(\Theta_{H_j}^{max}|\hat{\Psi}_{N_s})$. First, let's define an output error $e(n, \Theta_{H_j})$ as:

$$e(n, \Theta_{H_j}) = \hat{\psi}(n) - \psi(\Theta_{H_j}); \ \ n = 1, ..., N_s \qquad (13)$$

where $\hat{\psi}(n)$ is defined in Equation (3). Given Θ_{H_j}, an analytical data set $\psi(\Theta_{H_j})$ is defined similar to Equation (3):

$$\psi(\Theta_{H_j}) = \left[\mathbf{r}_1^T(\Theta_{H_j}), ..., \mathbf{r}_{N_r}^T(\Theta_{H_j})\right]^T \in \mathbf{R}^{N_t} \qquad (14)$$

It should be noted that a Ritz vector $\mathbf{r}_i(\Theta_{H_j})$ in Equation (14) has only the components associated with the measured DOFs.

Assuming each component of the output error $\{e_i(n, \Theta_{H_j}); n = 1, ..., N_s\}$ to be a multivariate normal distribution with zero mean and variance σ_i, the conditional joint PDF of Θ_{H_j} becomes:

$$f(\Theta_{H_j}|\hat{\Psi}_{N_s}) = f(e(n, \Theta_{H_j})|\hat{\Psi}_{N_s})$$
$$= k \cdot exp\left\{-J(\hat{\Psi}_{N_s}, \Theta_{H_j})\right\} \qquad (15)$$

where $k = \frac{1}{[2\pi]^{\frac{N_s}{2}}}\frac{1}{\|\mathbf{C}_{\hat{\Psi}}\|^{\frac{1}{2}}}$, $\|\mathbf{C}_{\hat{\Psi}}\| = det|diag[\sigma_1^2, ..., \sigma_{N_t}^2]| = \prod_{i=1}^{N_t} \sigma_i^2$, and the variance σ_i can be evaluated from observations of the estimated Ritz vector sets. When a large number of experimental data sets are available, sample standard deviations (or variances) can be extracted from the data sets. When modal data sets available are not sufficient to estimate the variances, we assign uniform coefficient of variance (COV) to all components of $e(n, \Theta_{H_j})$. Furthermore, the error function $J(\hat{\Psi}_{N_s}, \Theta_{H_j})$ is:

$$J(\hat{\Psi}_{N_s}, \Theta_{H_j}) = \qquad (16)$$
$$\frac{1}{2}\sum_{n=1}^{N_s} \left[\hat{\psi}(n) - \psi(\Theta_{H_j})\right]^T \mathbf{C}_{\hat{\Psi}}^{-1} \left[\hat{\psi}(n) - \psi(\Theta_{H_j})\right]$$

From Equations (4), (12) and (15), the upper bound of $P(H_j|\hat{\Psi}_{N_s})$ becomes:

$$P_U(H_j|\hat{\Psi}_{N_s}) = f(\Theta_{H_j}^{max}|\hat{\Psi}_{N_s})P(H_j)$$
$$= exp\left\{-J(\hat{\Psi}_{N_s}, \Theta_{H_j}^{max})\right\} \cdot P(H_j) \cdot k \qquad (17)$$

From Equation (17) and the fact that the relative comparison of $P_U(H_j|\hat{\Psi}_{N_s})$ is independent of the constant k, the following relationships hold:

$$\max\left[P_U(H_i|\hat{\Psi}_{N_s}), P_U(H_j|\hat{\Psi}_{N_s})\right] = \qquad (18)$$
$$\max\left[ln\, P_U(H_i|\hat{\Psi}_{N_s}), ln\, P_U(H_j|\hat{\Psi}_{N_s})\right] =$$
$$\min\left[J(\hat{\Psi}_{N_s}, \Theta_{H_i}^{max}) - lnP(H_i), J(\hat{\Psi}_{N_s}, \Theta_{H_j}^{max}) - lnP(H_j)\right]$$

where ln denotes a natural logarithm. Therefore, the most probable hypothesis H_{max} in Equation (5) satisfies:

$$J(\hat{\Psi}_{N_s}, \Theta_{H_{max}}^{max}) - lnP(H_{max})$$
$$= \min_{\forall H_j}\left[J(\hat{\Psi}_{N_s}, \Theta_{H_j}^{max}) - lnP(H_j)\right] \qquad (19)$$

Now, the comparison of posterior probabilities can be conducted by examining only the error function $J(\hat{\Psi}_{N_s}, \Theta_{H_j}^{max})$ and the prior probability $P(H_j)$.

A branch-and-bound search scheme is proposed to expedite the search for the most likely damaged substructure without exhaustively examining all the possible damage cases. Furthermore, sensitivities of Ritz vectors with respect to the stiffness change of a member is derived to measure the relative significance of the Ritz vectors to damages and a weighting scheme of Ritz vectors is proposed based on the derived sensitivity. For a detailed explanation of the branch-and-bound scheme and the sensitivity analyses, readers are referred to Reference [5, 4].

3   NUMERICAL EXAMPLES

An eight-bay truss structure from the NASA dynamic scale model technology (DSMT) program of Langley Research Center is employed to demonstrate the proposed approach (Figure 1). A detailed description of the example structure can be found in Reference [3]. Figure 2 shows the classification of the truss members into four different lacing patterns: longeron, batten, face diagonal and side diagonal. First, the sensitivities of the Ritz vectors are compared to those of modal vectors. Second, the damage detection of the eight-bay truss structure is conducted by changing damage locations, load patterns and damage thresholds. Furthermore, the damage detection using Ritz vectors are compared to the damage detection using modal parameters.

3.1 Sensitivity Analyses of Ritz Vectors

In this subsection, the sensitivities of Ritz vectors are compared with those of modal vectors. In the sensitivity analysis, load pattern 1 shown in Figure 3 (a) is employed for the generation of Ritz vectors. The sensitivity analysis is conducted by comparing the changes of the Ritz and modal vectors as the stiffness of each substructure (member) deteriorates. Selected results from the comparisons are presented in Figures 4, 5 and 6. Figure 4 (a) shows how the first five Ritz vectors change as the stiffness loss of the 33th member (a longeron in bay six) varies from 0% to 100%. For a simple graphical representation, the ratio of $\|\mathbf{r}_r^h - \mathbf{r}_r^d\|^2$ to $\|\mathbf{r}_r^h\|^2$ is computed to indicate the change of a Ritz vector as damage progresses in the 33th member. Here, $\| \cdot \|^2$ denotes the Euclidean norm and $\mathbf{r}^h$ and $\mathbf{r}^d$ denote the Ritz vectors before and after damage occurs, respectively. Figure 4 (b) shows similar quantities for the first five modal vectors, where $\mathbf{v}^h$ and $\mathbf{v}^d$ present the modal vectors before and after stiffness changes, respectively. The shaded portion of the plot indicates that if each component of a modal vector has a 5% of uncertainty level, no measurable change in any modal vector will be apparent unless the stiffness loss exceeds 75%. On the other hand, 10% change of stiffness results in perceivable changes in the second and third Ritz vectors in the presence of a 5% of uncertainty level. As a second example, Figure 5 presents the sensitivity comparison for the stiffness change of the 94th member (a side diagonal in bay six). While the fourth and fifth Ritz vectors are very sensitive to the stiffness change of the 94th member, the change of modal vectors is not apparent until the stiffness loss reaches about 40%. Figure 6 shows that the stiffness change of the face diagonal member 71 does not change the first five modal vectors at all and causes very little change in the Ritz vectors. Similar sensitivity results are observed for all face diagonal members.

From the sensitivity analyses conducted in this subsection, several observations can be made: (1) In most cases, stiffness changes in the model lead to larger changes in the Ritz vectors than in the modal vectors, (2) face diagonals do not cause significant changes to either the Ritz or modal vectors, and (3) in many cases, Ritz and modal vectors are more sensitive to the stiffness losses of side diagonals and longerons than those of battens.

3.2 Damage Detection of An Eight-Bay Truss

This subsection presents the diagnosis results of an eight-bay truss structure conducted under different conditions. For all examples, a uniform prior probability is assigned to all hypotheses. Therefore, the determination of the most probable hypothesis in Equation (19) depends only on the error function $J(\hat{\Psi}_{N_s}, \Theta_{H_j}^{max})$. The search space $\Theta_{H_j} < \Omega_{H_j}^*$ in Equation (7) is evaluated at the intersection of grid lines which discretize the search domain with an increment of $\Delta\theta$. For all numerical examples, we use an incremental step $\Delta\theta = 0.1$. The branch-and-

bound search in the presented examples follows a depth-first/best-first search strategy.

Ritz vectors are simulated following the generation procedure described in Reference [4] and each Ritz vector is normalized with respect to a reference point. The DOF which has the absolute maximum magnitude in each Ritz vector of the healthy structure, is assigned as a reference point. All the other DOFs are normalized with respect to this reference point. To simulate measurement uncertainties in the estimated Ritz vectors, the estimated Ritz vector set $\hat{\psi}(n)$ in Equation (3) is constructed such that:

$$\hat{\psi}(n) = \psi \left(1 + \frac{\mathcal{N}}{100} \mathcal{R}\right) \tag{20}$$

where ψ is the exact Ritz vector set obtained from the analytical model, $\mathcal{N}$ is a specified noise level in terms of percentage, and $\mathcal{R}$ is a normally distributed random number with zero mean and a variance of 1.0. This process is repeated N_s times to simulate the N_s data sets.

Excitation is assumed to be a swept sine excitation generated from electrodynamics or hydraulic shakers. All actuators are assumed to generate forces with the same magnitude and phase. The spatial distribution of forces is assumed not to vary with time. Load patterns are selected to maximize the sensitivities of the first five Ritz vectors over all substructures. However, a systematic scheme for the selection of load patterns is not considered here. For all examples, L_{dam} and D_{dam} denote the actual damage locations and the associated damage amount, respectively. $\hat{L}_{dam}$ and $\hat{D}_{dam}$ denote the most probable damage locations and the associated damage amount estimated by the proposed method. In Section 3.2.1, twelve damage cases with a single damage location are investigated using a uniform damage threshold for every substructure. Fourteen damage cases including the previous twelve damage cases are re-diagnosed in Section 3.2.2 using different damage threshold values for substructures. Finally, six damage cases with either two or three damaged substructures are examined in Section 3.2.3.

3.2.1 Using A Uniform Damage Threshold

In this subsection, twelve different damage cases are investigated employing Ritz vectors. For the purpose of comparison, the diagnosis results using modal vectors are also presented. Sensitivity analyses which are similar to Figures 4, 5 and 6, are conducted for load patterns 1 and 2 to define a minimum detectable damage. The *minimum detectable damage* of each substructure is defined as the minimum damage amount which the estimated Ritz vectors from a given load pattern can detect when each component of a Ritz vector is contaminated by a certain level of noise. The minimum detectable damage of each substructure is computed assuming that, because of noise, each component of a Ritz vectors is perturbed by 5% of its magnitude. Since it is shown that the detection of stiffness losses in most face diagonals and battens seems difficult from the assumed load patterns, the face diagonals and

battens are precluded from the branch-and-bound search in this subsection.

In Table 4, twelve damage cases with a single damaged substructure are simulated by assuming a 10% stiffness loss, a 5% noise level and one data set (N_s=1). The damaged substructures used in the examples are shown in Figure 1 by solid lines. Furthermore, all DOFs are assumed to be measured and a value of 0.9 is used for the damage threshold θ^* of each substructure.

For all damage cases, the most probable damage events computed by the proposed method include the actually damaged substructure. In some cases, however, undamaged substructures are also included in the most probable damage event. For example, the 7th substructure is included as a potentially damaged substructure in case A. This is due to the fact that the Ritz vectors employed in this diagnosis set (the Ritz vectors generated from load pattern 2) are insensitive to the stiffness changes of the 7th substructure. Therefore, a small stiffness change of the 7th substructure may not result in a noticeable change of the error function value in Equation (16) or actually can reduce the error function value when Ritz vectors are noise contaminated. For similar reasons, the 5th substructure is also included in the most probable damage event for other damage cases. The rank of the actual damage event, estimated using the first five modal vectors, is presented in parenthesis of the third column of Table 4. The table shows that the first five modal vectors fail to locate the actual damage locations in most cases.

3.2.2 Using Different Damage Thresholds

In this subsection, fourteen damage cases (including the previous twelve cases) are diagnosed using a different threshold value for each substructure. The other conditions are unchanged (Noise=5%, N_s=1 and all DOFs are measured). We prevent unnecessary extensions of the proposed branch-and-bound search by employing preliminary sensitivity analyses. The branch-and-bound search is conducted including only substructures with damage larger or equal to the pre-assigned minimum detectable damage. The diagnoses in previous subsection show that Ritz vectors have different sensitivities for different substructures. This observation motivates the use of a different threshold for each substructure. The damage thresholds in this subsection are assigned based on the minimum detectable damage. For example, when the minimum detectable damage amount assigned to a substructure is 20%, the corresponding damage threshold is set to 0.8. It should be noted that when the total removal of a substructure does not cause a perceivable change in Ritz vectors, the substructures are defined as undetectable and excluded from the diagnosis. For example, the 67th member (face diagonal in bay one) is defined as undetectable since the total removal of the member (100% stiffness loss) does not yield significant changes in Ritz vectors beyond the assumed variation cause by uncertainties. Therefore, the 67th member is excluded from the diagnosis.

Table 5 shows that the redefined damage threshold improves the diagnoses. Comparing the most probable events (hypothesis) of case A in Tables 4 and 5, one can observe that the undamaged 7th substructure is removed from the most probable hypothesis, making the actual damage case the most probable one. In case E, the proposed method indicates that most likely there is no damage. Considering the fact that the damage threshold of the 36th substructure is set to 0.2, the 10% stiffness loss in the 36th substructure is not detectable. The proposed method ranks the 36th substructure as the 17th most probable damage location with 80% damage. Similar results are observed for cases F and M. A sensitivity analysis shows that the stiffness deterioration of the 71th substructure, which is a face diagonal in the 7th bay, does not yield any noticeable changes to the estimated Ritz vectors. Therefore the 71th substructure is precluded from the diagnosis and the proposed method provides a false-negative indication of damage. For case M, the damage threshold of the 17th substructure is set to 0.8. Again the proposed method indicates that most likely there is no damage and ranks the event of 20% damage in the 17th substructure as the 9th most probable damage case.

3.2.3 Diagnoses of Damage in Multiple Locations

In this subsection, we focus on the detection of damage in multiple locations. Table 6 presents diagnosis results of six different damage cases. In cases O $\sim$ R, 10% stiffness decrease is simulated in two substructures. Cases S and T introduce 10% stiffness reduction in three substructures. The six damage cases are repeatedly diagnosed under different conditions. In the third column of Table 6, the first five Ritz vectors are generated from load pattern 1 and employed for damage detection. In the fourth column, load pattern 2 is employed instead of load pattern 1. In the last column of the table, a total of ten Ritz vectors are generated from load patterns 1 and 2 (the first five Ritz vectors are generated from each load pattern). For all cases in Table 6, all DOFs are measured and one set of Ritz vectors is simulated assuming a 5% noise level (N_s=1 and Noise=5%).

When the first five Ritz vectors are generated from load pattern 1, the proposed method identifies the actual damage event of cases O, P, Q and T. However, the actual damage locations are not detected for cases R and S. While the use of load pattern 2 yields the detection of actual damage locations in cases P, Q and R, load pattern 2 fails to identify damage of cases O, S and T. Finally, when a total of ten Ritz vectors are generated from load patterns 1 and 2, the proposed method identifies the actual damage locations for all cases. It is shown that each damage case has different sensitivity to different load patterns and by including more Ritz vectors from different load

patterns, diagnosis results can be improved.

4 CONCLUSIONS

This study incorporates load-dependent Ritz vectors, as an alternative to modal vectors, into a Bayesian probabilistic framework for damage detection. Load-dependent Ritz vectors have potential superiority over modal vectors in that (1) in general, load-dependent Ritz vectors are more sensitive to damage than the corresponding modal vectors, (2) by a careful selection of load patterns, substructures of interest can be made more observable using the Ritz vectors generated from the particular load patterns, and (3) while the extraction of higher modes is difficult, a larger set of Ritz vectors can be estimated by imposing different load patterns.

References

[1] J. L. Beck, M. W. Vanik, and L. S. Katafygiotis. Determination of stiffness changes from modal parameter changes for structural health monitoring. In *The Proceedings of The First World Conference on Structural Control*, Pasadena, CA, 1994.

[2] T. T. Cao and D. C. Zimmerman. A procedure to extract Ritz vectors from dynamic testing data. In *The Proceeding of the 15th International Modal Analysis Conference, Orlando, FL*, pages 1036–1042, 1997.

[3] T. A-L. Kashangaki. Ground vibration tests of a high fidelity truss for varification of on orbit damage location techniques. Technical Report NASA-TM-107626, National Aeronautics and Space Administration, 1992.

[4] H. Sohn and K. H. Law. Application of load-dependent Ritz vectors to Bayesian probabilistic damage detection. *Submitted for publication*, 1997.

[5] H. Sohn and K. H. Law. Bayesian probabilistic approach for structure damage detection. *Earthquake Engineering and Structural Dynamics (in press)*, 1997.

Table 4: Comparison of Diagnoses Using Ritz or Modal Vectors

| Case | Actual Damage | | | Most Prob. Dam. | |
	L_{dam}	Rank[1]	$\hat{L}_{dam}$	$\hat{D}_{dam}$
A	{46}	3/313(350/434)[2]	{7,46}	{80%,10%}
B	{102}	1/251(30/434)	{102}	{10%}
C	{39}	3/313(350/434)	{7,39}	{80%,10%}
D	{97}	3/313(55/434)	{5,97}	{80%,10%}
G	{33}	2/313(372/434)	{5,33}	{30%,10%}
H	{35}	3/313(219/434)	{5,35}	{80%,10%}
I	{94}	3/313(356/434)	{5,94}	{70%,10%}
J	{28}	3/313(382/434)	{5,28}	{80%,10%}
K	{87}	1/251(405/434)	{87}	{10%}
L	{22}	3/313(320/434)	{5,22}	{80%,10%}
M	{17}	3/313(428/494)	{5,17}	{70%,10%}
N	{3}	3/313(213/494)	{3,5}	{10%,70%}

1. The first number is the rank of the actual damage event and the second is the total number of the examined hypotheses.
2. The rank in the parenthesis is estimated using the first five modal vectors.
3. N_s=1, Noise=5%, all DOFs are measured, and 10% stiffness reduction is assumed for all damage locations. The first five Ritz vectors are estimated from load pattern 2.

Table 5: Diagnoses Using Different Threshold Values

Case	Actual Damage		Most Prob. Damage		
	L_{dam}	D_{dam}	Rank[1]	$\hat{L}_{dam}$	$\hat{D}_{dam}$
A	{46}	{10%}	1/371	{46}	{10%}
B	{102}	{10%}	1/552	{102}	{10%}
C	{39}	{10%}	1/371	{39}	{10%}
D	{97}	{10%}	1/461	{97}	{10%}
E	{36}	{10%}	17/95	No Damage	
F	{71}	{10%}	-/95	No Damage	
G	{33}	{10%}	1/371	{33}	{10%}
H	{35}	{10%}	1/461	{35}	{10%}
I	{94}	{10%}	1/462	{94}	{10%}
J	{28}	{10%}	1/371	{28}	{10%}
K	{87}	{10%}	1/371	{87}	{10%}
L	{22}	{10%}	1/461	{22}	{10%}
M	{17}	{10%}	9/95	No Damage	
N	{3}	{10%}	1/461	{3}	{10%}

1. The first number is the rank of the actual damage event and the second is the total number of the examined hypotheses. "-" denotes that actual damage is not detected.
2. The first five Ritz vectors are estimated from load pattern 2.
3. N_s=1, Noise=5%, and all DOFs are measured.
4. Different damage threshold is assigned to each substructure.

Table 6: Diagnoses of Multiple Damage Locations

Case	L_{dam}	Rank		
		F1[1]	F2[2]	F1, F2[3]
O	{35,94}	1/672	-/371	1/686
P	{39,46}	1/483	1/644	1/686
Q	{28,102}	1/861	2/914	1/974
R	{39,87}	-/672	1/644	1/679
S	{22,35,97}	-/672	-/644	1/686
T	{17,35,97}	1/577	-/554	1/986

1. The first five Ritz vectors are estimated from load pattern 1.
2. The first five Ritz vectors are estimated from load pattern 2.
3. Load Patterns 1 and 2 are employed and the first five Ritz vectors are estimated from each load pattern.
4. N_s=1, Noise=5%, and all DOFs are measured.
5. Different damage threshold value is assigned to each substructure.
6. 10% of stiffness reduction is assumed for all damaged substructures.
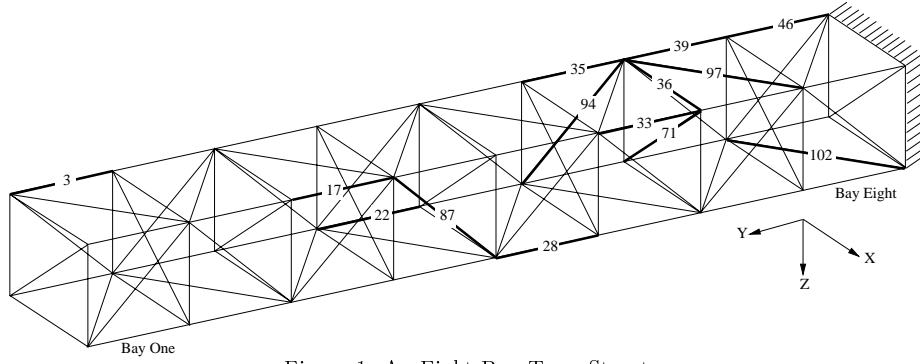
Figure 1: An Eight-Bay Truss Structure
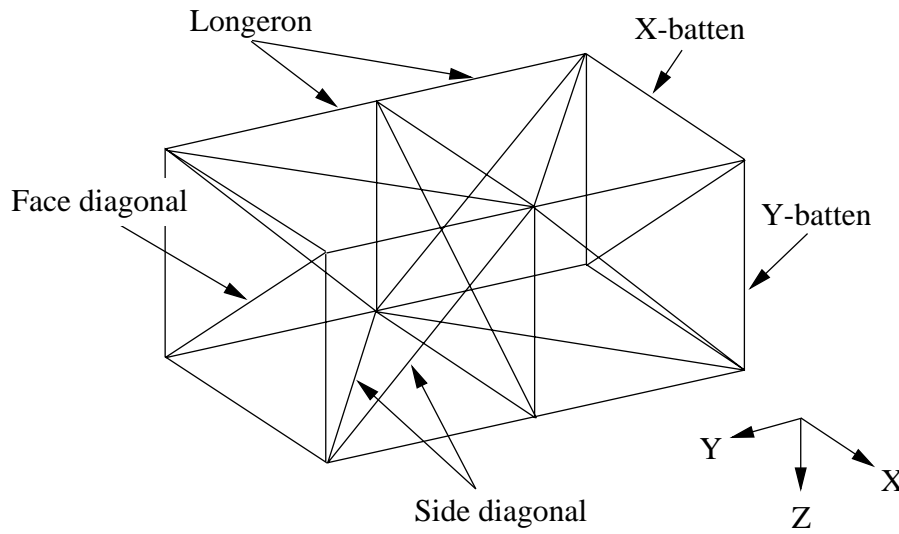
Figure 2: Lacing Patterns of An Eight-Bay Truss Structure

(a) Load Pattern 1
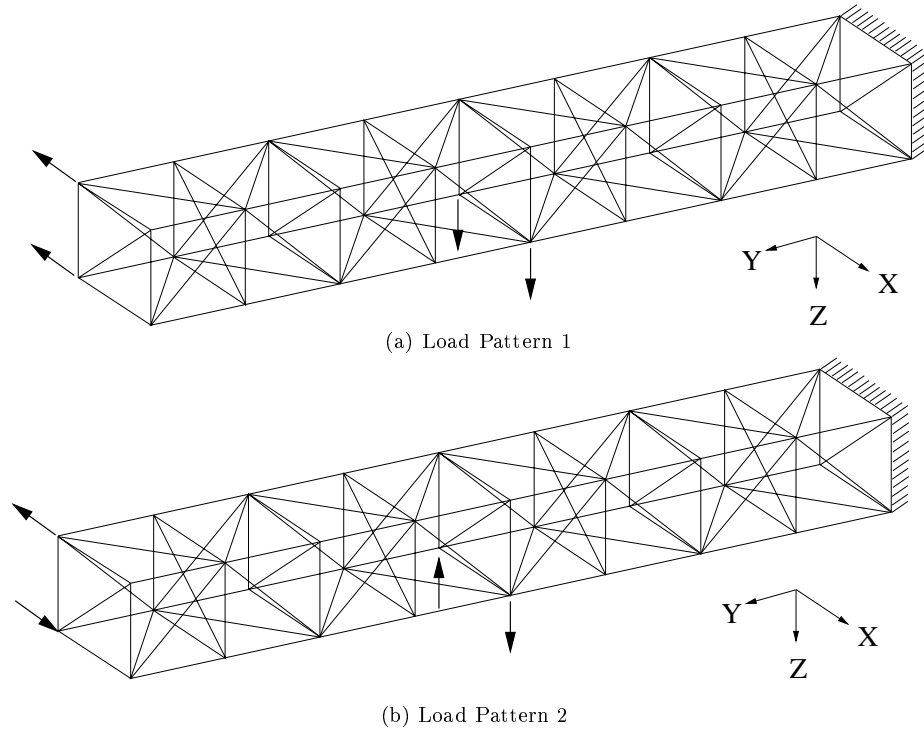
(b) Load Pattern 2

Figure 3: Load Patterns Applied to An Eight-Bay Truss Structure
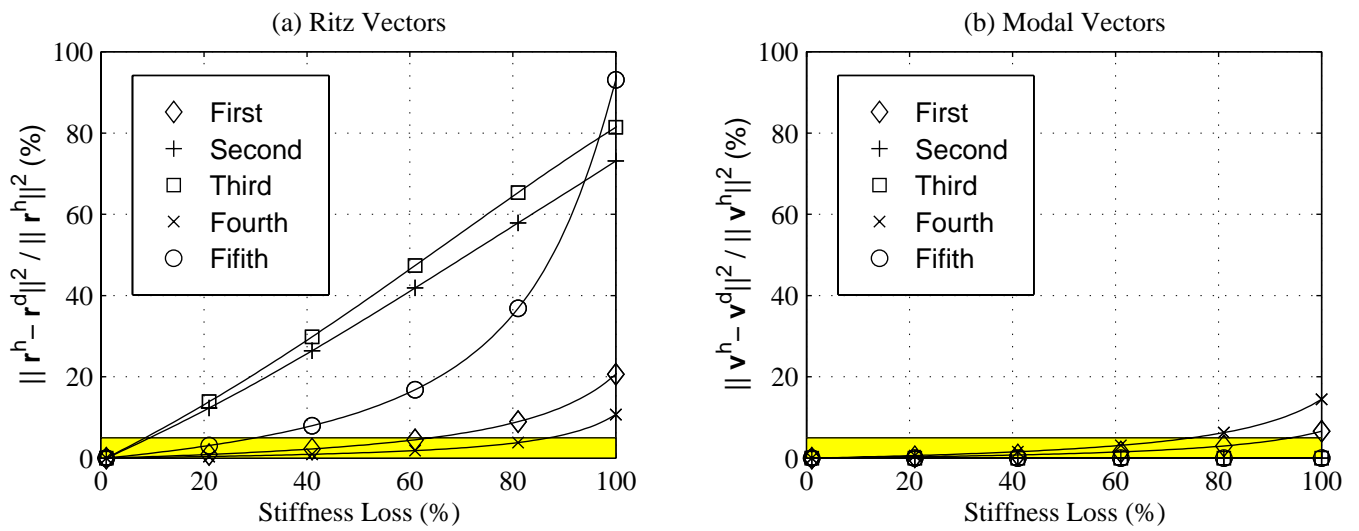
Figure 4: Sensitivity Comparison of Ritz and Modal Vectors for Progressive Damage in Member 33
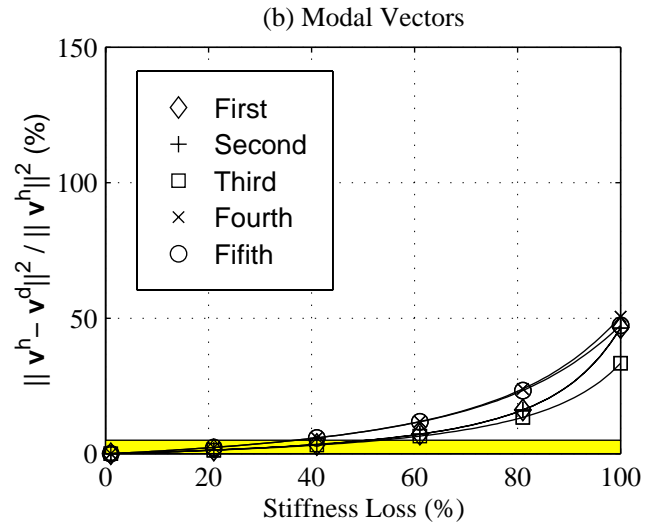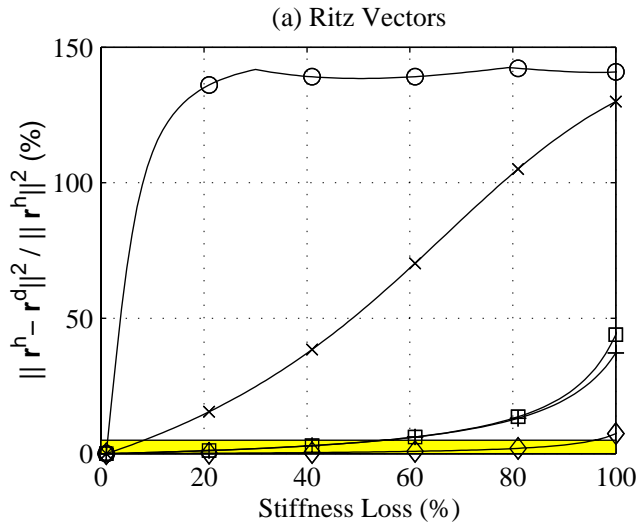
Figure 5: Sensitivity Comparison of Ritz and Modal Vectors for Progressive Damage in Member 94
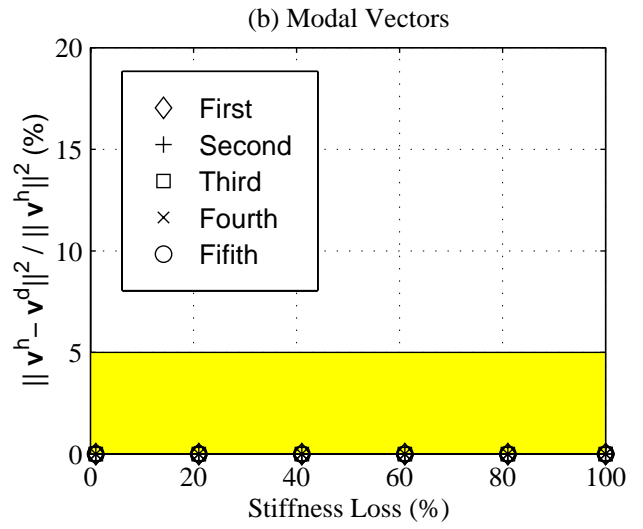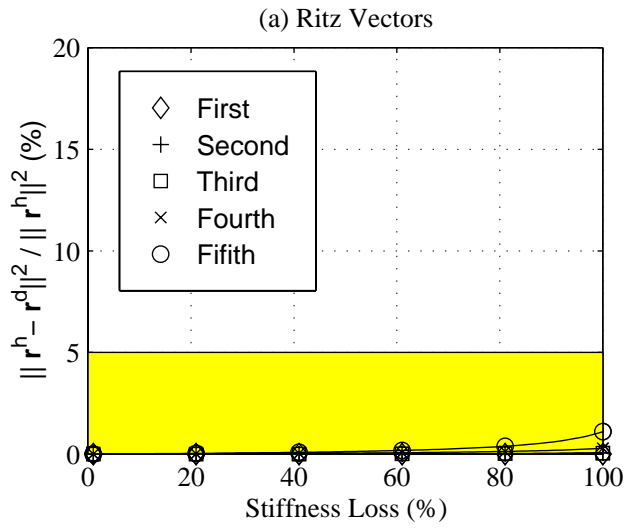
Figure 6: Sensitivity Comparison of Ritz and Modal Vectors for Progressive Damage in Member 71